

# Microstructure and electrical characteristics of shock-consolidated ZnO-Bi<sub>2</sub>O<sub>3</sub>-MnO<sub>2</sub> bulk

Youngkook Kim<sup>\*</sup>, Seong-Seung Kang<sup>\*\*</sup>, and Chai-Bong Lee<sup>\*\*\*†</sup>

<sup>\*</sup>Shock Wave and Condensed Matter Research Center, Kumamoto University  
2-39-1 Kurokami, Kumamoto City, Kumamoto, 860-8555, Japan

<sup>\*\*</sup>Department of Energy and Mineral Resources Engineering, Chosun University  
375 Seosuk-dong, Dong-gu, Gwangju 501-759, South Korea

<sup>\*\*\*</sup>Department of Electronics Engineering, Dongseo University  
San69-1, Jurye-2dong, Sasang-gu, Busan 617-716, South Korea  
Phone +82-51-320-1755

<sup>†</sup>Corresponding address : lcb@gdsu.dongseo.ac.kr

Received : March 22, 2012 Accepted : April 13, 2012

## Abstract

Consolidation of ZnO-Bi<sub>2</sub>O<sub>3</sub>-MnO<sub>2</sub> powders was performed using an underwater shock compaction technique. The compact exhibited crack-free formation, and interparticle bonding between ZnO powder particles was observed. Microstructure and peak broadening behavior of the compact was investigated by FE-SEM and X-ray analysis. Electric resistance was measured using the Nyquist plot method. The broadened peaks formed by lattice defects were detected in X-ray analysis, and high electric resistance of Mega ohms due to crystal deformations by shock energy was confirmed.

**Keywords** : underwater shock compaction, lattice defects, crack, ZnO

## 1. Introduction

ZnO-based varistors have been investigated extensively in response to their increasing demand as surge absorbers in electronic circuits and electric power systems. These devices exhibit highly nonlinear current-voltage characteristics utilized to limit voltage transients. Typical formulations of ZnO varistors comprise zinc oxide with minor additives categorized as varistor formers (Bi<sub>2</sub>O<sub>3</sub>, V<sub>2</sub>O<sub>5</sub>, Pr<sub>6</sub>O<sub>11</sub>)<sup>1-3)</sup> and assistant additives (Sb<sub>2</sub>O<sub>3</sub>, Cr<sub>2</sub>O<sub>3</sub>, MnO<sub>2</sub>)<sup>4), 5)</sup>. While varistor formers are essential for inducing the varistor behavior, assistant additives are added to increase nonlinear coefficient value. The nonlinear response of ZnO-based varistors is a grain boundary phenomenon, and thus, electrical characteristics are directly related to the size of ZnO grains<sup>2), 6), 7)</sup>.

The processing technique for the fabrication of varistors is critically important for the production of good varistors, and various techniques<sup>8)-12)</sup> have been developed for their fabrication. The most commonly used technique is sintering, in which the compact is exposed to a particular

temperature for a prolonged time<sup>10)</sup>. Conditions not properly controlled may lead to grain growth, resulting in inferior properties. For varistor fabrication, where grain growth is critical issue, shock compaction is a viable alternative.

Shock compaction<sup>13)</sup> is a one-stage densification process which occurs in a micro-second duration of time. No sintering is required for the post compaction process, and grain growth may thus be inhibited. Underwater shock compaction<sup>12), 14)-16)</sup> is a variation of this technique, in which water is used as a shock propagation medium. Use of this technique allows uniform shock pressure to be applied to powders over a longer period of time, leading to greater interparticle bonding. Underwater shock compaction has been used to fabricate ceramic materials with improved properties. In this investigation, ZnO-Bi<sub>2</sub>O<sub>3</sub>-MnO<sub>2</sub> based varistors were produced using underwater shock compaction, and their properties were studied.

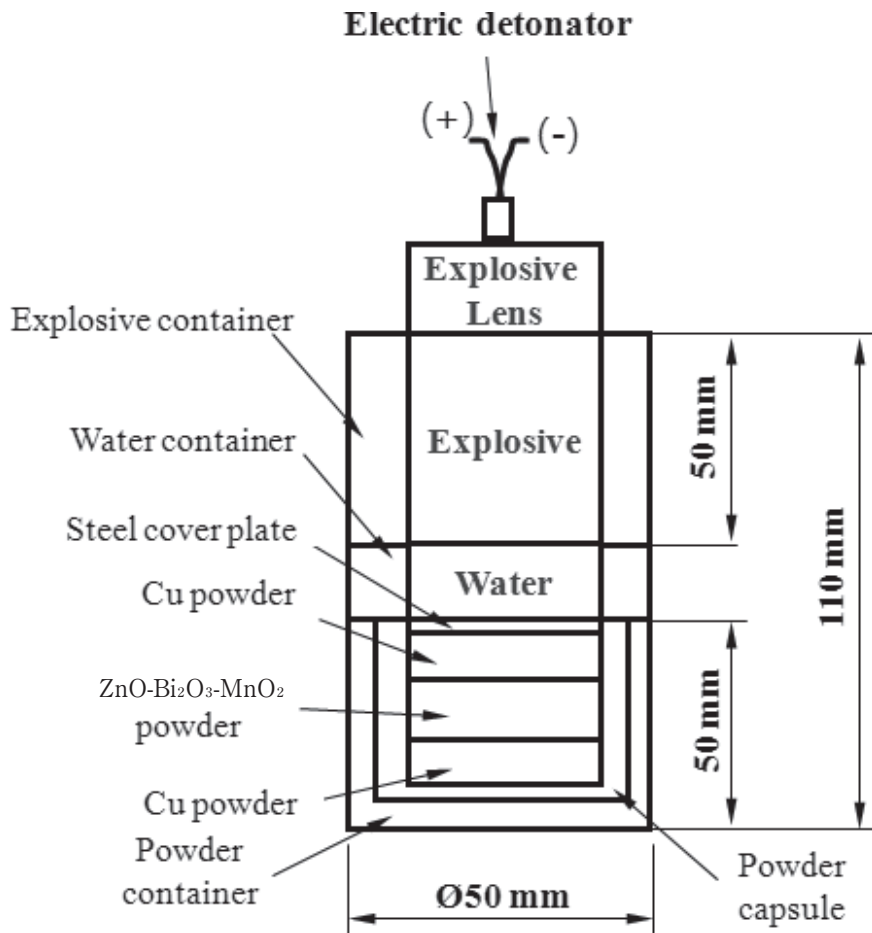


Figure 1 Schematic illustration of shock compaction device using underwater shock wave.

## 2. Experimental Procedure

In the present study, ZnO powders (Wako Chemical Co. Ltd., Japan) with an average size of  $\leq 2\mu\text{m}$  were doped with  $\text{Bi}_2\text{O}_3$  powder ( $\leq 5\mu\text{m}$  size, 0.5 mass%) and  $\text{MnO}_2$  powder ( $\leq 5\mu\text{m}$  size, 0.5 mass%). The powders were mixed by ball milling method for 3 hours with 100 rpm using a stainless steel container and alumina balls. Synthesis of the composite was carried out using underwater shock compaction as illustrated schematically in Figure 1. The assembly typically consisted of four parts: explosive container, water container, powder container and powder capsule. A high explosive, SEP (Kayaku Japan Co. Ltd, Japan), of detonation velocity 6.97 km/s and density 1300  $\text{kg/m}^3$ , was used to generate the shock pressure. In order to generate a planar shock wave, an explosive lens made of two types of explosives, SEP and HABW (Detonation velocity: 4.75 km/s and Density: 2200  $\text{kg/m}^3$ , supplied by Kayaku Japan Co. Ltd, Japan) was placed at the top of the explosive container. A water container with 10 mm height and 30 mm inner diameter was used to propagate the underwater shock wave. Distribution of the shock pressure was to be uniform and shock wave pulse duration increased, allowing more time for interparticle bonding. The powder capsule was placed below the water container and was filled with powders in three layers: the top and the bottom layers were copper powder with respective thicknesses of 15 mm and 6 mm; the middle layer was ZnO powder. The copper powder layers served two purposes: one, to prevent the spalling effect and thus

avoid compact cracking; and two, to decrease the rapid cooling time of the shock consolidated material. A stainless steel cover plate of 1 mm thickness was set on the top of the powder container in order to prevent penetration of impurities into the powder. Prior to consolidation, the powders were pressed by a uniaxial press machine for a theoretical density of 60%.

Field emission-scanning electron microscopy (FE-SEM, JSM-7600F, Japan) was used to observe the microstructure of the starting powders and the subsequent shock consolidated compact. The density was used measured by Archimedes method, and the electrical resistance was assessed by Nyquist plot method using a commercial impedance analyzer (HIOKI 3532-80 Chemical Impedance Meter).

## 3. Results and discussion

Figure 2 (a) is a photograph of the cross-sectioned powder capsule after shock compaction. No observable macroscopic defects can be seen along the cross section. This shows the ability of the underwater shock compaction technique to produce ZnO-based ceramics with no processing defects. The shock consolidated sample was cut into an elliptical shape with a width of 25 mm and thickness of 4 mm, as shown in Figure 2 (b). No cracks were formed during the processing, showing that the sample was able to withstand the mechanical vibrations. This indicates that the sample possesses adequate strength for practical applications. It is worth noting that,

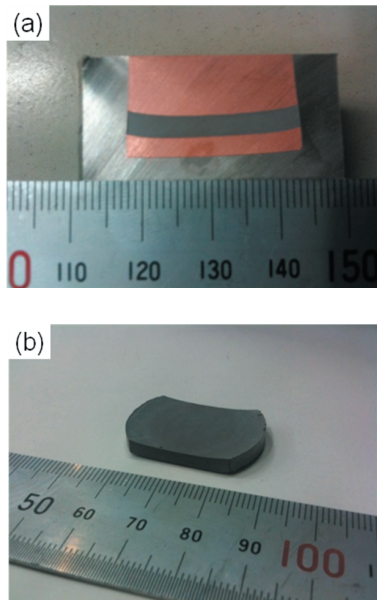


**Figure 2** Photographs of (a) shock-consolidated ZnO-Bi<sub>2</sub>O<sub>3</sub>-MnO<sub>2</sub> in the powder capsule and (b) processed shock-consolidated ZnO-Bi<sub>2</sub>O<sub>3</sub>-MnO<sub>2</sub>.

during shock compaction, cracks may be generated by the shock energy and residual tensile stresses<sup>13,15</sup>. The generation of cracks is prevented by the placement of copper powder above and below the ceramic. The residual heat from both powder layers retards the cooling of the compact and thus avoids inducement of thermal cracks on the ceramic sample.

The density of the shock compacted sample was measured by Archimedes principle, which showed relative density 98% of theoretical density. This high density achieved by the composite is due to the passage of the shock wave.

Figure 3 shows FE-SEM images of the fracture surface of shock consolidated ZnO-Bi<sub>2</sub>O<sub>3</sub>-MnO<sub>2</sub>. Relatively larger particles of Bi<sub>2</sub>O<sub>3</sub> and MnO<sub>2</sub> can be seen in Figure 3(a). A magnified microstructure of the ZnO particles on the fracture surface is shown in Figure 3(b). It can be observed that the powders were substantially deformed by the shock energy to fill the voids. Interparticle bonding between the particles is evident, and particle size as that of the starting powders is retained. In general, during shock compaction process, the propagation of the shock wave causes a powder particle to undergo plastic deformation and interparticle melting contributes to bonding. The behavior of shock-consolidated ceramics may differ depending on particle size. Large particles undergo particle fracture due to highly inhomogeneous stresses existing within the particles and the activation of existing flaws by tensile stresses, while small particles undergo plastic deformation. In the present work, the particles are small, and thus interparticle melting played a major role in the bonding. Bi<sub>2</sub>O<sub>3</sub> particles play an important role for ZnO-Bi<sub>2</sub>O<sub>3</sub>-based varistors. They usually provide the medium for liquid-phase sintering on grain boundaries and improve stability of nonlinear current-voltage characteristics<sup>17</sup>. Particles do not undergo phase change from solid to liquid during shock compaction.

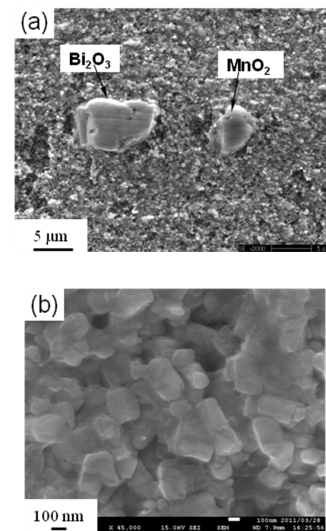


**Figure 3** Microstructure images of (a) shock-consolidated ZnO-Bi<sub>2</sub>O<sub>3</sub>-MnO<sub>2</sub> and (b) its detailed microstructure.

Therefore, to obtain a completely enveloped Bi<sub>2</sub>O<sub>3</sub> phase on the grain boundaries of ZnO, the mass percentage of Bi<sub>2</sub>O<sub>3</sub> should be increased. A better measured mass percentage of the particles and an appropriate particle size would improve the nonlinear characteristics.

Elemental mapping of the shock processed sample is shown in Figure 4. A reasonably homogeneous distribution of the elements can be seen in the microstructure. This is attributed to the combined effect of mechanical milling and shock compaction. Mechanical milling aids to distribute particles homogeneously and to form fine grains, while shock compaction allows retaining grain size during the bonding process. Though the distribution of bismuth and manganese elements are scattered due to their low percentage in the overall composition, the distributions of oxygen and zinc are reasonably homogeneous.

XRD (X-ray diffraction) patterns of the starting powders and the shock-consolidated ZnO-Bi<sub>2</sub>O<sub>3</sub>-MnO<sub>2</sub> are displayed in Figure 5. The results indicate that ZnO was the main phase and that additives were not observed as they constituted a small fraction of the overall composition. In comparison with the pattern of the starting powders, the shock-consolidated sample displays broadened peaks. This is attributed to a decrease of crystalline size. However, similarity in peak pattern indicates that no chemical reaction or phase change occurred during the shock compaction process.

Figure 6 shows Nyquist diagram of shock-consolidated ZnO-Bi<sub>2</sub>O<sub>3</sub>-MnO<sub>2</sub>. It is well known that grain boundaries play an important role in electrical resistivity. The Nyquist plot method was often used to study about the electrical resistivity of bulk ZnO ceramics<sup>18,19</sup> and the impedance spectrum was measured by electric current flow with increasing frequency. In the Nyquist plot measurement, the sample was used as a square bulk shape with the size of 5 mm×5 mm×1 mm (thickness). The electrical response of the sample was estimated with increasing frequency ranging from 600 Hz up to 1 MHz. In the figure, the linear part indicates the resistivity of the electrode, and the

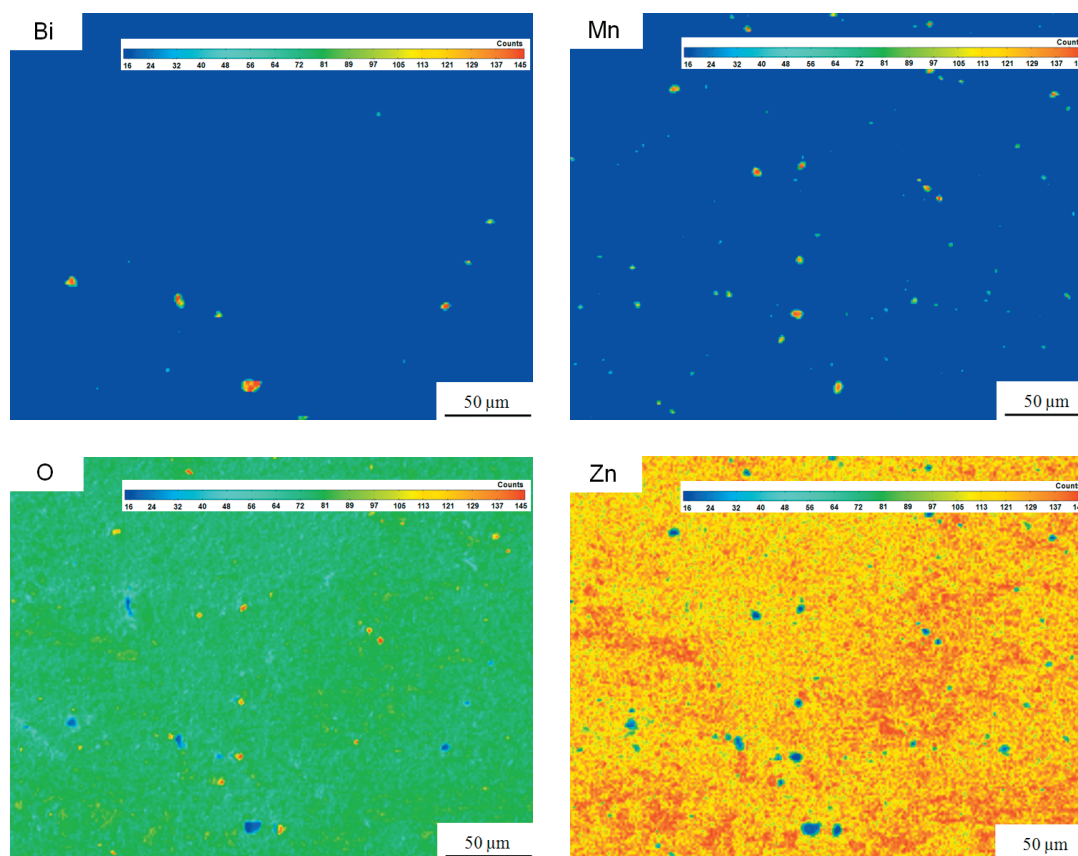


Figure 4 EPMA images of shock-consolidated ZnO-Bi<sub>2</sub>O<sub>3</sub>-MnO<sub>2</sub>.

curve part is derived from the grain boundary barrier and grain barrier. Figure 6 shows that grain boundary resistivity of the shock-consolidated sample was in the range of Mega-ohms. This value is significantly higher than commercially processed ZnO samples<sup>15</sup>. The shock energy caused a large amount of grain boundaries in the shock processed sample, contributing to an increase in grain boundary resistivity. It is worth repeating that electrical characteristics of varistors are controlled by the grain boundary barriers. Thus, a fine-grained structure with minimal presence of mechanical defects such as voids and cracks introduced by shock compaction is ideal for a varistor<sup>20</sup>.

A varistor microstructure should remain homogenous with regard to the nature and distribution of phases; this dictates the processing strategy employed to obtain the ceramic powder.

Varistor ceramics with inhomogeneous microstructure can cause a large spread in current-voltage characteristics due to high local currents, leading to degradation of the varistor during electrical operation. Intensive milling by a ball mill allows for homogeneous distribution of dopants and a decrease in grain size; it also allows for more refined particles with a fine microstructure, which is beneficial to the electrical properties of the varistors. However, retaining the fine grained microstructure during processing of the ceramic remains crucial, and as the shock compaction process occurs in a very short time, it avoids the excessive grain growth which is detrimental to the properties of the ceramic.

#### 4. Conclusions

ZnO-Bi<sub>2</sub>O<sub>3</sub>-MnO<sub>2</sub> bulk was fabricated by underwater shock compaction. Crack-free formation was confirmed on the ceramic sample, possible because of the presence of Cu powders which retarded the rapid cooling process of the ceramic compact. In the microstructure, interparticle bonding between ZnO powder particles was observed, and powders were seen to have been substantially deformed by the shock energy, thus filling voids. Broadened peaks were detected in all phases, and high electric resistance was confirmed due to an increase in grain boundaries, lattice defects and deformation of crystallite by shock energy. The Bi<sub>2</sub>O<sub>3</sub> particles did not undergo phase change from solid to liquid phase; such a phase change would lead to a decrease in the efficacy of Bi<sub>2</sub>O<sub>3</sub> distributed on the grain boundaries. In conclusion, underwater shock compaction has shown itself to be a good technique for obtaining fine-structured grains without grain growth, although it has proven difficult to distribute the Bi<sub>2</sub>O<sub>3</sub> phase which can induce the stability of the nonlinear current-voltage characteristics. Therefore, an appropriate mass percentage of Bi<sub>2</sub>O<sub>3</sub> for binding ZnO particles and an appropriate particle size would improve the nonlinear characteristics.

#### Acknowledgements

This work was supported in part by the Research Funds of Innovative Collaboration Organization of Kumamoto University in Japan.

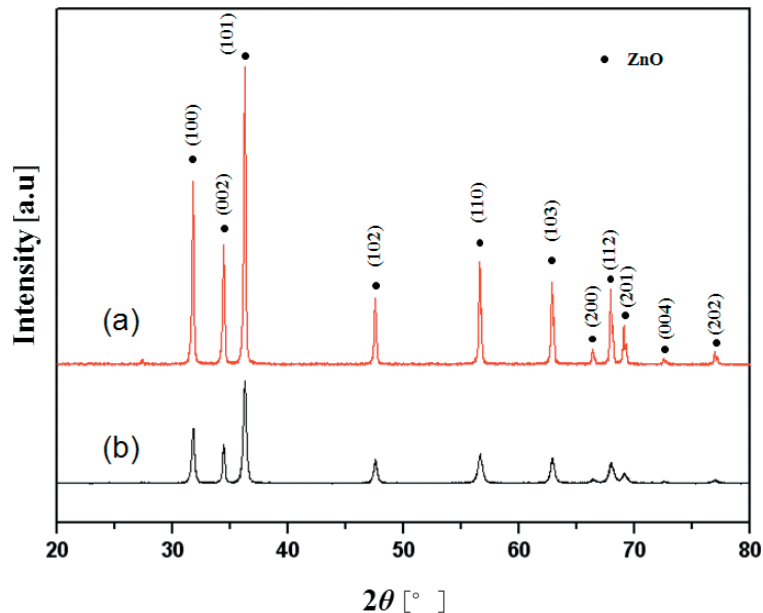


Figure 5 X-ray diffraction peaks of (a) ZnO-Bi<sub>2</sub>O<sub>3</sub>-MnO<sub>2</sub> starting powder and (b) shock-consolidated ZnO-Bi<sub>2</sub>O<sub>3</sub>-MnO<sub>2</sub>.

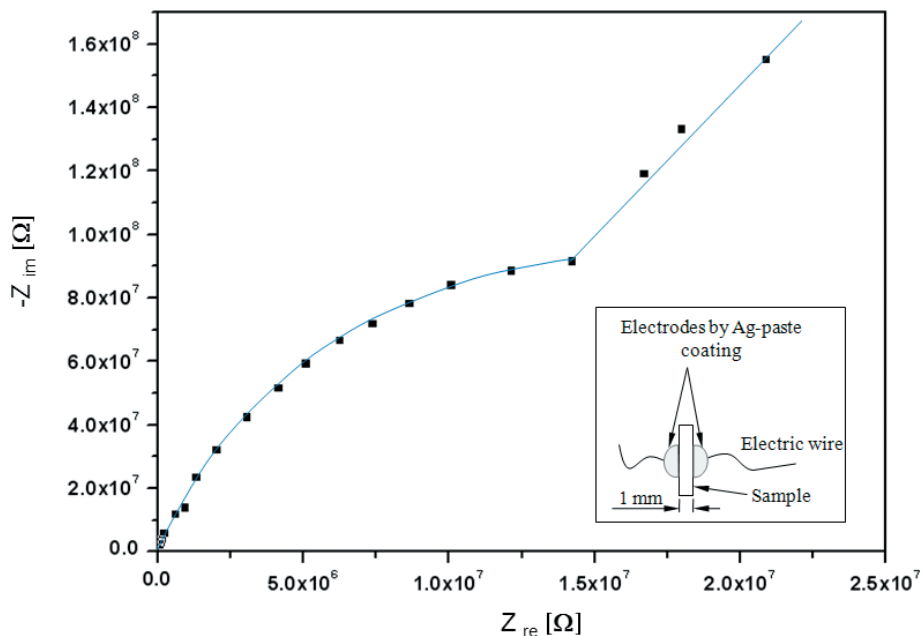


Figure 6 Nyquist plot of shock-consolidated ZnO-Bi<sub>2</sub>O<sub>3</sub>-MnO<sub>2</sub>.

## References

- 1) S. Anas, R. Metz, M.A. Sanoj, R.V. Mangalaraja and S. Ananthakumar, *Ceram. Inter.* 36, 2351–2358 (2010).
- 2) H. H. Hng and L. Halim, *Mater. Lett.* 57, 1411–1416 (2003).
- 3) C. W. Nahm and H. S. Kim, *Mater. Lett.* 57, 1544–1549 (2003).
- 4) J. Wu, C. Xie, J. Hu, D. Zeng and A. Wang, *J. European Ceram. Soc.* 24, 3635–3641 (2004).
- 5) C. Zhang, Y. Hu, W. Lu, M. Cao and D. Zhou, *J. European Ceram. Soc.* 22, 61–65 (2002).
- 6) T. O. Özkan, M. Avci, E. Oktay and H. Erkalpa, *Ceram. Inter.* 24, 151–156 (1998).
- 7) S.T. Kuo and W. H. Tuan, *J. European Ceram. Soc.* 30, 525–530 (2010).
- 8) C. Leacha, N. K. Ali, D. Cupertino and R. Freera, *Mater. Sci. Eng. B* 170, 15–21 (2010).
- 9) J. Zhang, S. Cao, R. Zhang, L. Yu and C. Jing, *Current Appl. Phys.* 5, 381–386 (2005).
- 10) J. K. Tsai and T. B. Wu, *Mater. Lett.* 26, 199–203 (1996).
- 11) T. Asokan, *Mater. Res. Bull.* 28, 1277–1284 (1993).
- 12) Y. Kim, I. Tomoaki and S. Itoh, *Powder Technol.* 208, 575–581 (2011).
- 13) M. A. Meyers, D. J. Benson and E. A. Olevsky, *Acta mater.* 47, 2089–2108 (1999).
- 14) Y. Kim, F. Mitsugi, I. Tomoaki, K. Hokamoto and S. Itoh, *J. European Ceram. Soc.* 31, 1033–1039 (2011).
- 15) Y. Kim, T. Ueda, K. Hokamoto and S. Itoh, *Ceram. Inter.* 35, 3247–3252 (2009).
- 16) A. Chiba, S. Kimura, K. Raghukandan and Y. Morizono, *Mater. Sci. Eng. A* 350, 179–183 (2003).
- 17) D. Xu, X. N. Cheng, X. H. Yan, H. X. Xu and L. Y. Shi, *Trans. Nonferrous Met. Soc. China* 19, 1526–1532 (2009).
- 18) J. L. Ning, D. M. Jiang, K. H. Kim and K. B. Shim, *Ceram. Inter.* 33, 107–114 (2007).
- 19) F. M. Filho, A. Z. Simoes, A. Ries, L. Perazolli, E. Longo and J. A. Varela, *Ceram. Inter.* 32, 283–289 (2006).
- 20) L. Wang, G. Tang and Z. K. Xu, *Ceram. Inter.* 35, 487–492 (2009).